Research Square

Preprints are preliminary reports that have not undergone peer review.
They should not be considered conclusive, used to inform clinical practice,
or referenced by the media as validated information.

Cyclic Strombolian Activity at Etna Volcano: Insights From the November–December 2023 Eruptive Episode

Luciano Zuccarello

luciano.zuccarello@ingv.it

Istituto Nazionale di Geofisica e Vulcanologia, Sezione di Pisa

Duccio Gheri

University of Liverpool

Silvio De Angelis

University of Liverpool

Mariangela Sciotto

Istituto Nazionale di Geofisica e Vulcanologia

Gabriela Badi

Universidad Nacional de La Plata

Article

Keywords:

Posted Date: May 15th, 2026

DOI: https://doi.org/10.21203/rs.3.rs-9619616/v1

License: This work is licensed under a Creative Commons Attribution 4.0 International License.
Read Full License

Additional Declarations: No competing interests reported.

Cyclic Strombolian activity at Etna volcano: insights from the November–December 2023 eruptive episode

Luciano Zuccarello[1,2,*], Duccio Gheri[2], Silvio De Angelis[2,1], Mariangela Sciotto[3], and Gabriela Badi[4]

[1]Istituto Nazionale di Geofisica e Vulcanologia, Sezione di Pisa, Via Cesare Battisti, 53, 56125 Pisa, Italy.
[2]School of Environmental Sciences, University of Liverpool, 4 Brownlow Street, Liverpool L69 3GP, UK.
[3]Istituto Nazionale di Geofisica e Vulcanologia, Sezione di Catania - Osservatorio Etneo, Piazza Roma, 2, 95125 Catania, Italy.
[4]Centro de Investigaciones Geofísicas, Facultad de Ciencias Astronómicas y Geofísicas, Universidad Nacional de La Plata, Paseo del Bosque s/n, 1900 La Plata, Buenos Aires, Argentina.
[*]corresponding author luciano.zuccarello@ingv.it

ABSTRACT

Lava fountains are typical of basaltic volcano eruptions, especially during paroxysms when activity shifts from intermittent Strombolian explosions to sustained, high lava discharge, often with ash emission. Cyclic eruptive behaviour - marked by regular variations in explosive intensity and lava fountaining over minutes to hours - has been observed before but rarely captured in the geophysical record. In November 2023, Mt. Etna (Italy) exhibited remarkably cyclic activity, culminating in a paroxysm on 1 December, 2023. Over 10 days, clusters of rapid explosions lasting 15–20 minutes recurred every 50–70 minutes from multiple vents in the South East Crater. Infrasound data show repetitive waveforms, indicating consistent eruption dynamics and discharge volumes across cycles. Seismic tremor locations point to a shallow source within the uppermost kilometer beneath the crater. This activity is interpreted as resulting from episodic collapse of gas-rich magmatic foam trapped at shallow depth in the conduit. The activation of multiple, sometimes short-lived vents suggests branching of conduit pathways, likely driven by repeated fracturing in the more crystalline upper crater layer. These observations provide new insight into Etna's shallow eruptive processes and support models linking cyclic explosive behaviour in basaltic volcanoes to near-surface gas accumulation and release.

Introduction

Basaltic volcanoes exhibit a spectrum of eruptive behaviours, ranging from lava effusion to discrete Strombolian explosions and, occasionally, transitions to paroxysmal activity characterized by sustained, high-flux, lava discharge events (i.e., lava fountains) accompanied by the injection of volcanic ash in the atmosphere[1,2]. These common manifestations of eruptive activity at basaltic volcanoes can overlap or occur sequentially, driven by magma ascent, accumulation, and degassing within the shallow conduit (e.g.,[3–5]). Open-vent volcanoes, like Mt. Etna (Italy), offer natural laboratories to investigate transitions between discrete, semi-continuous, Strombolian activity and more energetic paroxysmal events[6]. The frequency and character of these transitions are primarily controlled by the efficiency and style of gas-magma separation during ascent[7]. Lava flows are typically associated with the extrusion of low-viscosity, degassed magma[8], while Strombolian explosions arise from the rapid ascent and bursting of gas bubbles of varying sizes, formed by volatile exsolution at depth within the magma column or storage region[9]. At the lower end of the energy spectrum lies spattering activity, which is linked to a bubbly flow regime[10]. In contrast, more energetic events occur when gas bubbles grow to the diameter of the conduit, and a transitioning into the slug flow regime[11] occurs. Upon reaching the surface, these slugs burst in different scenarios, ranging from simple bubble bursting at the free magma surface to explosive rupture following the failure of a tensile-strength-bearing plug in the uppermost part of the conduit system[12–14]. An increase in gas volume fraction within the conduit may shift the flow regime from slug to annular flow[11,15], potentially leading to sustained lava fountaining. This transition can be triggered by two primary mechanisms: (i) an increase in magma ascent rate and volatile flux, leading to progressive bubble coalescence throughout the conduit[16], or (ii) massive foam collapse at the reservoir depth, resulting in a rapid gas release and subsequent annular flow[17].

Both Strombolian explosions and lava fountaining may exhibit cyclic or pulsatory patterns, although this type of behavior has rarely been captured in geophysical datasets. The 2021 eruption of the Fagradalsfjall volcano in Iceland represents one of the very few documented examples of periodic and repetitive lava fountaining episodes. Through analyses of gas chemistry and eruption dynamics[18], proposed a model in which changes in shallow magma chamber overpressure controlled the cyclic nature of the eruption.

Despite these advances, robust geophysical documentation of cyclic Strombolian behavior at Etna has remained elusive. Here we present a remarkable sequence of cyclic Strombolian eruptive activity at Etna volcano, recorded during November–December 2023. This cyclic behavior is completely different from other cyclic phenomena documented at Etna, such as the seismic and tremor cyclicity observed in 2008–09[19], the main difference being that in those cases, no clear surface manifestations accompanied the subsurface cyclic patterns. During the 2023 sequence, the volcano produced highly regular, time-clustered Strombolian explosions from its South East Crater (Fig. 1a); clusters of explosions lasted 15–20 minutes and recurred regularly every 50–70 minutes over a period of 10 days. The cyclic activity culminated in a paroxysm on 1 December 2023.

The geophysical signature of these eruptive cycles was captured by the extensive seismic and acoustic monitoring network (Fig. 1b) of the Istituto Nazionale di Geofisica e Vulcanologia (INGV), yielding an exceptional dataset to investigate eruption dynamics. We analyze the characteristics of the seismic and acoustic records in both the time and frequency domains, identify the source region of continuous volcanic tremor, and track systematic variations in the character of explosions and seismo-acoustic energy release associated with transitions in eruption style (e.g.,[20]). These observations provide new insights into cyclic Strombolian activity, shallow conduit dynamics, and the processes leading to paroxysmal transitions. Our results highlight the key role of shallow conduit conditions in controlling eruptive variability, where the interplay between ascending gas and transient near-vent structures modulates degassing and explosion dynamics. Progressive pressurization within the upper conduit drives the transition from discrete explosive activity to more sustained eruptive phases, ultimately leading to abrupt shifts in eruption style.

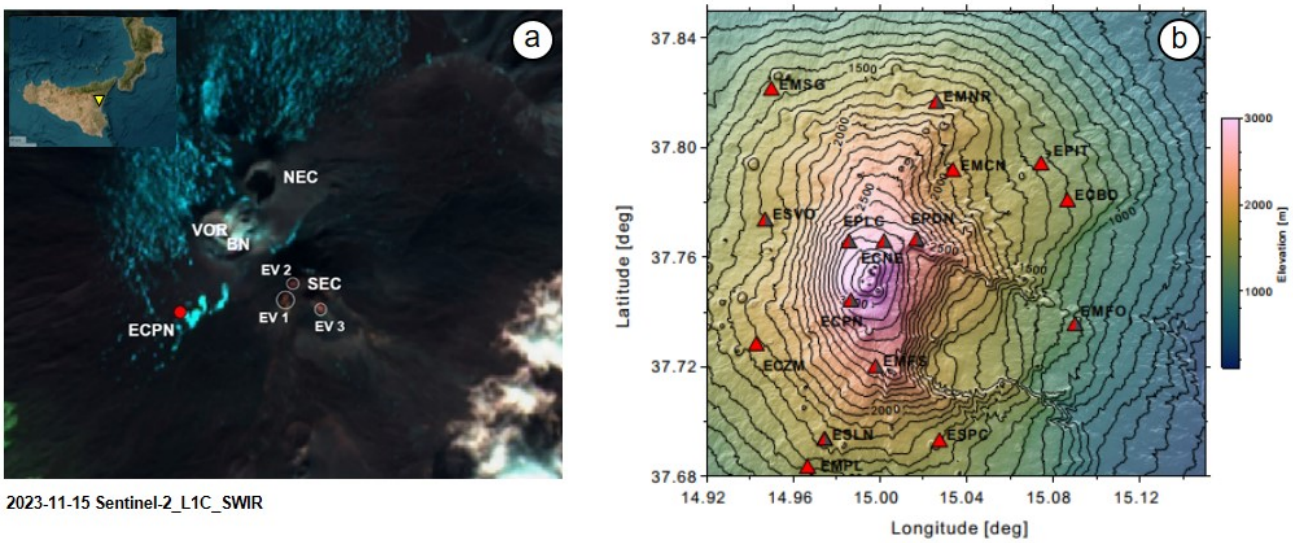


Figure 1. (a) Map of the summit craters (BN, Bocca Nuova; VOR, Voragine; NEC, North East Crater; SEC, South East Crater; NSEC, New South East Crater) at Mt. Etna, including a detail of the three active ephemeral vents (EV) within the South East Crater, as observed in Sentinel-2 L1C SWIR image, and the position of ECPN seismo-acoustic station. The inset map shows the location of Mt. Etna (yellow triangle) on the island of Sicily, southern Italy; (b) Configuration of part of the INGV-OE seismo-acoustic permanent network used in this study. Triangles indicate station locations: red triangles represent seismic stations, while red and grey triangles denote seismo-acoustic stations.

Results

Pre-paroxysm cyclic activity

Cyclic Strombolian activity during 20-30 November, 2023 and the paroxysm on 1 December, 2023 were captured by INGV seismic and infrasound stations in the proximity of the summit crater area of Mt. Etna (Fig. 1a). Eruptive activity throughout the study period remained confined to the South East Crater (SEC), where explosions produced pyroclastic ballistics reaching heights 150–200 meters above the rim. The bulk of explosive and fountaining activity was linked to a primary vent in the western part of SEC, while a secondary vent located to the east generated modest ash emissions quickly dispersed by summit winds. Occasionally, the more active western vent also produced short-lived lava overflows along the southwestern flank. Several ephemeral vents were observed to form throughout the study period producing emissions ranging from continuous active degassing to ash-rich explosions (Fig. 1a; see also Supplementary Fig. S1). Bocca Nuova (BN) was also moderately

active during the study period, primarily exhibiting persistent background degassing occasionally interrupted by discrete overpressure outbursts. In contrast, activity at other summit craters remained largely unchanged: the North East Crater (NEC) exhibited only minor intra-crater degassing and Voragine (VOR) showed no signs of activity[21].

Figure 2 shows the seismo-acoustic time series of the eruptive activity at Etna between November 20 and December 3, 2023, based on ECPN station (Fig. 1a). Throughout the observation period, a continuous background tremor was recorded, with seismic energy primarily concentrated in the 0.5–7 Hz frequency range (Fig. 2a). Periodic increases in RSAM amplitude (closely spaced peaks), particularly evident in the seismic data (Fig. 2b), correlate with Strombolian episodes and culminate in a sharp and intense peak during the paroxysmal lava fountaining event on December 1. It is worth noting that as the Strombolian episodes grew in magnitude leading up to the paroxysmal event as well as the background noise in the data also increased.

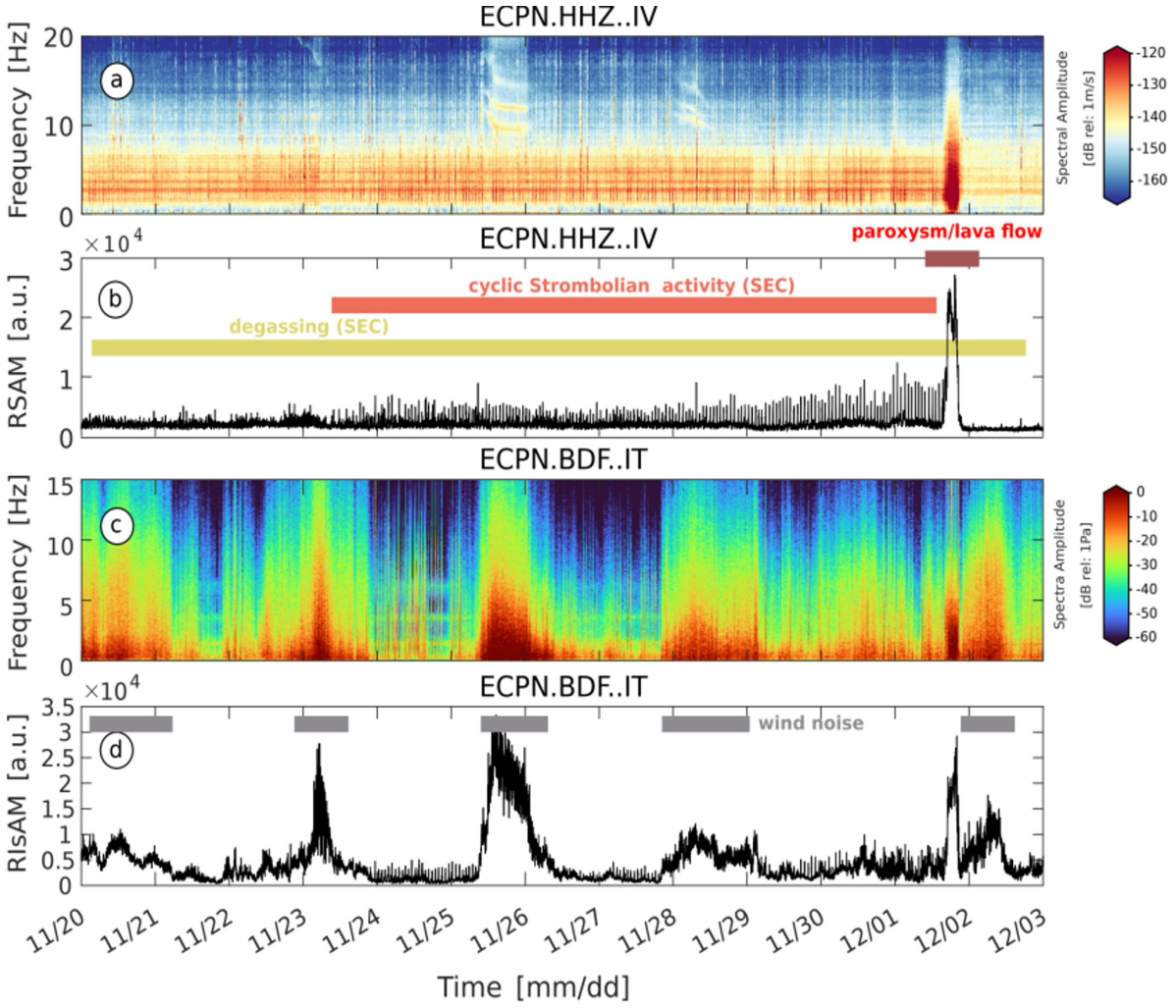


Figure 2. Seismo-acoustic characterization of the eruptive activity at Etna from November 20 to December 3, 2023, based on data from the ECPN stations. a) Seismic spectrogram showing continuous background tremor and distinct spectral bands associated with Strombolian explosions and the final paroxysm. b) Root Mean Square Amplitude (RSAM) of seismic data, highlighting cyclic energy fluctuations and a sharp amplitude peak during the paroxysmal event on December 1. c) Infrasound spectrogram displaying regularly spaced, high-energy pulses that correspond to individual explosive events. d) RSAM of infrasound data, illustrating the periodicity and intensity of Strombolian episodes; wind noise periods are also indicated.

The main feature observed in the spectrogram of the seismic signal is a well-defined spectral band between 2 and 4 Hz, together with the presence of clearly distinguishable harmonics, which are characteristic of volcanic tremor at Etna during degassing activity[19]. A distinctive aspect of the analyzed signal lies in the occurrence of a secondary seismic source, manifested by the presence of individual transients superimposed on the harmonic spectrum with a regularity that is also evident in the RSAM of the seismic signal. These transients, with frequencies reaching up to 20 Hz, can be attributed to Strombolian

explosions recorded during the study period, as confirmed by surveillance cameras operated by INGV-OE[21]. This superposition persisted throughout the analysis interval and ceased immediately after the paroxysmal event of December 1.

A similar pattern is observed in the infrasound data (Fig. 2c,d). During periods of lower wind intensity (Fig. 2d), the acoustic spectrogram reveals regularly spaced, high-energy pulses that align with the seismic peaks, corresponding to explosive phases (Fig. 2c). The RSAM computed from the infrasound signal clearly highlights this cyclicity, with distinct peaks due to the Strombolian episodes. A sharp and persistent peak was observed during the paroxysm that occurred at 17:15 UTC on December 1st[21], due to the intense and sustained eruptive activity.

Seismic tremor localization

Volcanic tremor is a key monitoring parameter at Mount Etna, reflecting magma migration and surface processes that constrain eruption style and timing. Long recognized as a proxy for magma transport and a precursor of eruptive activity (e.g.,[22–28]) , tremor can be exploited to investigate subsurface magma dynamics relevant to hazard forecasting. We adopted amplitude-based methods, which estimates source positions from amplitude decay without requiring identifiable P- or S-wave phases. To estimate the tremor centroid at Etna, we applied a grid-search procedure based on the spatial distribution of Seismic Amplitudes, assuming body-wave propagation in a homogeneous medium[29–31]. The analysis targeted the 0.5–2.5 Hz frequency band, the same routinely used by INGV Osservatorio Etneo to track tremor source migrations[32,33]. Location uncertainties, quantified with the jackknife method (see Methods for further details about the algorithm and technique), averaged 0.6 km (longitude), 0.6 km (latitude), and 1.0 km (altitude), consistent with previous estimates (e.g.,[32,34]).

Figure 3a,b shows the spatial and temporal distribution of the centroid of the volcanic tremor source. The source is observed to cluster within the shallow portion of plumbing system of Etna (e.g.,[21]), in a position consistent with the main feeding system of the summit craters and extending along the primary conduit toward the eastern sector of the summit area[35]. Significant temporal variations in source depth are evident. During the cyclic phase (20–31 November), the centroid remains located at approximately 1.5 km above sea level (green dots, Fig.3a,b). Before this interval, as well as after the December paroxysm, the tremor source shows a migration along the main feeding system. This pattern indicates that the source follows a branching geometry, consistent with the structure of the shallow plumbing system previously identified at Etna (e.g.,[36]). The vertical distribution of the source is characterized by fluctuations over time (Fig. 3a,b). During periods of cyclic activity, the source stabilizes at shallow levels, whereas outside these intervals it exhibits a broader range of depths along the principal feeding system. These observations are in agreement with earlier geophysical and geochemical (e.g.,[37–40]) studies that constrain the position of a shallow storage or trapping zone at Etna. In particular, relatively high CO2/SO2 ratios measured in intra-eruptive quiescent gas emissions from the summit craters (e.g.,[41]) support the occurrence of shallow bubble accumulation at depths of 1–2 km a.s.l., consistent with the centroid locations retrieved here.

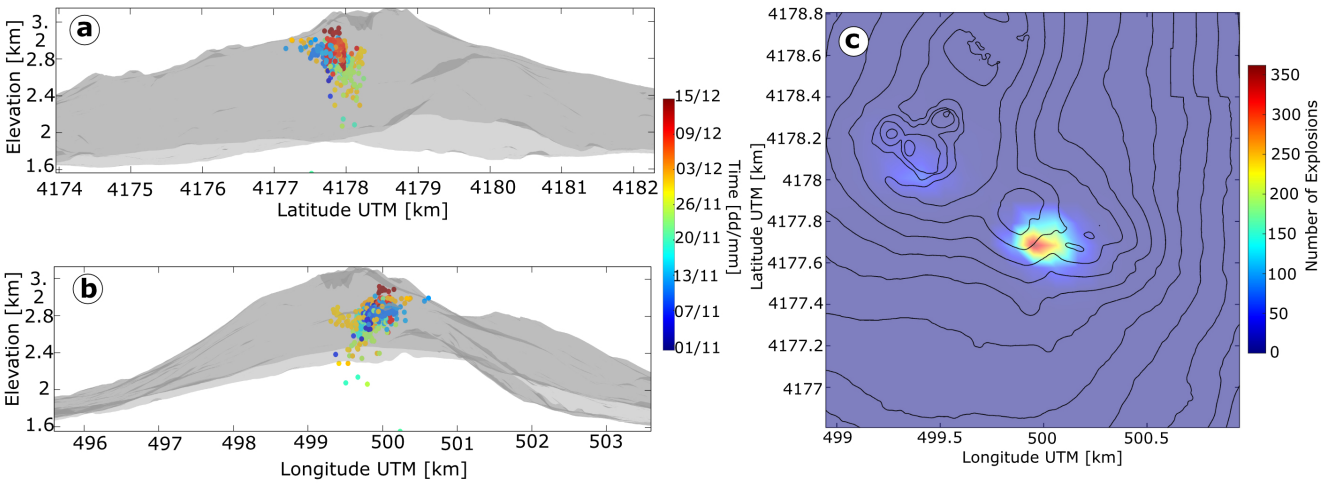


Figure 3. (a,b) Cross-sectional views of the volcanic tremor source positions beneath the summit area of Mt. Etna, shown as projections onto the latitude–elevation and longitude–elevation planes, respectively. Tremor source locations are colour-coded according to their time of occurrence. (c) Map view of the summit craters showing the spatial density of localized infrasound explosions. Colours indicate the number of explosions per grid cell. The highest concentration of infrasound events is located at the SE Crater, with a secondary cluster at Bocca Nuova.

Infrasound explosions localization

Volcanic infrasound at Mt. Etna is generally composed of discrete events lasting from less than one second to more than thirty seconds (e.g.,[42,43]). These signals are typically marked by impulsive compression onsets and well-defined spectral peaks, with most of the acoustic energy concentrated in the 0.3–6.0 Hz frequency band[33]. Continuous monitoring is carried out by the permanent infrasonic network operated by INGV, Osservatorio Etneo – Sezione di Catania. The spatial origin of individual events is inferred through a grid-search method that applies the brightness function to locate the source (e.g.,[33,44]). During the investigated period, all infrasound sources were consistently localized within the sector encompassing the BN and SEC craters. The spatial distribution of events indicates a strong predominance of activity at the SEC, with a substantially smaller contribution from BN. Event detection and localization were systematically carried out by the monitoring network operated by INGV-OE (see Methods for details on the processing workflow). In total, more than 1,600 discrete infrasound events were identified. Of these, approximately 1,300 events were spatially attributed to SEC, while around 300 were associated with BN. The spatial density of localized events is illustrated in Figure 3c, where maxima are clearly observed above the active craters, particularly in correspondence of SEC. The temporal distribution of infrasound detections further highlights that SEC was characterized by persistent, cyclic explosive activity throughout the observation window (Supplementary Fig. S2), where infrasound explosion counts are reported as a function of time). This eruptive pattern continued without interruption until the onset of the paroxysmal phase on 1 December. Intervals characterized by apparent gaps in event localization are not interpreted as reflecting a cessation of eruptive activity. Instead, these intervals are attributed to temporary degradation in detection capability, most likely caused by enhanced ambient noise levels linked to wind effects, which decreased the signal-to-noise ratio of the recorded waveforms. By exploiting the localization results of individual infrasound detections, we extracted representative waveform signatures of Strombolian explosions originating specifically from the SEC crater. This dataset enabled a robust characterization of the temporal organization of the eruptive cycles, including their recurrence intervals and waveform structure, thereby providing key constraints on the dynamics of explosive activity at SEC during the analyzed period.

Cyclic explosive activity at SEC was continuous throughout the analysis period (Fig. 5), persisting until the onset of the paroxysm on December 1. The apparent gaps in event localization during some intervals are not attributed to a pause in eruptive activity, but rather to increased background noise, most likely due to the effect of wind, which reduced the signal-to-noise ratio.

By exploiting the localization results of individual infrasound events, we were able to extract the waveform signatures of the Strombolian explosions specifically associated with the SEC crater. This enabled a detailed characterization of the temporal structure and recurrence of the eruptive cycles.

Strombolian activity

To characterize the cyclic Strombolian activity, we focused on the time window from November 24, 09:00 UTC to November 25, 06:00 UTC, during which wind conditions were minimal and the signal-to-noise ratio of the infrasound data was particularly high (Fig. 4). This period of low-intensity wind allowed for clear identification and extraction of individual explosive events.

Figure 4ab-cd shows the seismic and infrasonic waveforms and spectrograms, respectively, for the selected period at ECPN station. A strong correspondence between acoustic peaks and seismic features is evident, particularly in the spectral content. The acoustic pulses exhibit a frequency range comparable to that of the seismic signal (0.5–7 Hz, Fig. 4bd). Notably, the cyclicity of the explosions is more clearly resolved in the infrasound waveforms, whereas in the seismic data, it is partly obscured by the continuous background tremor.

To further investigate the cyclic nature of the Strombolian activity, we identified individual explosive cycles based solely on the localizations of infrasonic events occurring at the SEC crater. Each cycle consists of a sequence of discrete explosions, and for each identified cycle we computed the onset and end times, the duration of the active phase (i.e., the interval between the first and last explosion within a cluster), the inter-cycle recharge time (defined as the time between the end of one cycle and the onset of the next), the number of explosions, the peak acoustic pressure, and the cumulative Volume Eruptive Rate (VER), following the methodologies of[45,46]. In total, 19 complete cycles were identified. On average, the active phase lasted 22.8 $\pm$ 14.3 min and each cycle comprised 43.7 $\pm$ 24.0 explosions, with a mean onset-to-onset recurrence time of 62.9 $\pm$ 15.4 min.

Figure 5a shows an extract of the infrasonic pressure signal, where individual cycles are easily distinguishable as clusters of explosions. Yellow and blue markers denote the start and end times of each cycle, respectively. The parameters derived for each cycle are shown in panels 5b–e. Peak pressure values remain broadly consistent through time (mean = 24.3 $\pm$ 7.0 Pa; Fig. 5b), whereas cumulative VER shows a wider spread, averaging $2.99 \times 10^4 \pm 1.90 \times 10^4$ m^3/s (Fig. 5c). Recharge times average 39.4 $\pm$ 14.5 min and, when compared with peak pressure and cumulative VER (Fig. 5d–e), display moderate variability but no clear trend, suggesting a regularity in the magma supply and pressurization at shallow depth.

In this period, we extracted and stacked 878 individual infrasound events filtered between 0.1 and 10 Hz (Fig. 5f). The resulting average waveform (in red) shows a distinctive signature, characterized by a rapid compressional onset followed by a longer, lower-amplitude rarefaction phase - typical of mild Strombolian explosions.

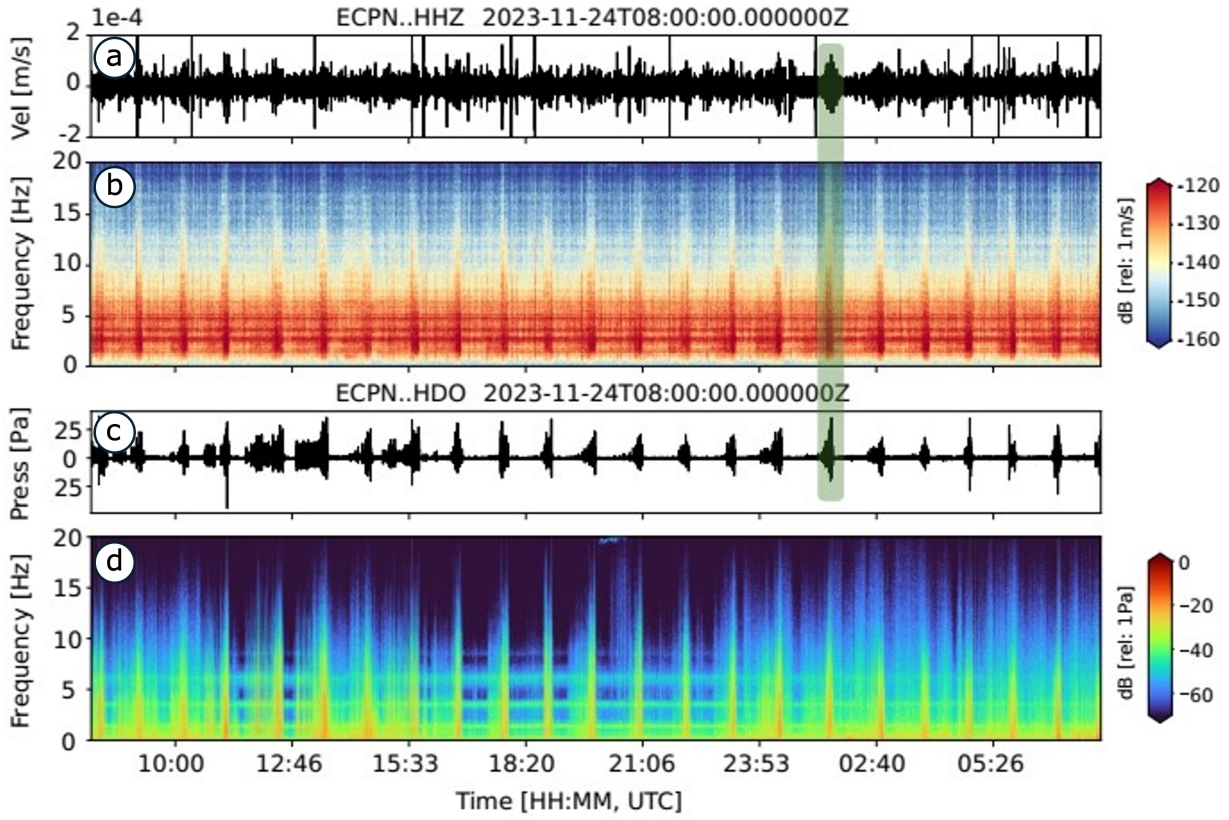


Figure 4. a) Seismic signals b) spectrogram c) infrasound signals d) infrasound spectrogram. d) infrasound stacking d) cycle characterization expressed in terms of mean peak frequency, number of explosions, and tremor amplitude, coloured coded according to the normalised time.

To explore the internal evolution of each explosive cycle, we performed a 4-minute moving window analysis with a 1-minute overlap, extracting the number of explosions and their mean peak pressure within each time window. The analysis was applied to all identified cycles, and the results are presented in Supplementary Figure S2.

A consistent intra-cycle pattern is evident: as time progresses within each cycle (i.e., as color shifts from blue to red), there is a systematic increase in the number of explosions, infrasound peak pressure, and seismic RSAM amplitude. This means that each cycle follows a repeatable internal evolution, where explosive activity intensifies towards the end of the cycle.

Discussion

Our observations provide the first robust data evidence that theoretical models describing magma–gas dynamics in the shallow feeding system are consistent with the paroxysmal manifestations at Mount Etna. In particular, we document cyclic Strombolian activity that persisted for about ten days before culminating in a paroxysmal lava fountain at the South East Crater (SEC). The cyclic character of the explosive gas release, and its distinctive features within each cycle, reflect variable physical conditions in the shallow conduit. These findings, when considered together with existing models for basaltic volcanoes, allow us to outline a conceptual framework (Fig. 6) that accounts for both the cyclic activity and the observed transitions across multiple active vents at the SEC.

The eruptive cyclicity is characterized by 20±2 min bursts of Strombolian explosions separated by 60-70 min repose intervals, indicating a regular and episodic gas supply from depth. Both peak infrasound pressure and volcanic explosion rate (VER) show little variation with recharge time (Fig. 5), consistent with steady-state degassing and stable conduit dynamics. Despite this overall stability, significant temporal variations in source depth are observed (Fig.3a,b). The vertical distribution of these sources can be attributed to magma dynamics processes, including magma ascent, accumulation of magmatic gases, and bubble coalescence leading to the formation of a foam layer[15,29]. This interpretation is consistent with previously proposed models of conduit degassing at Etna, which invoke the formation and collapse of a gas-rich foam layer within the plumbing

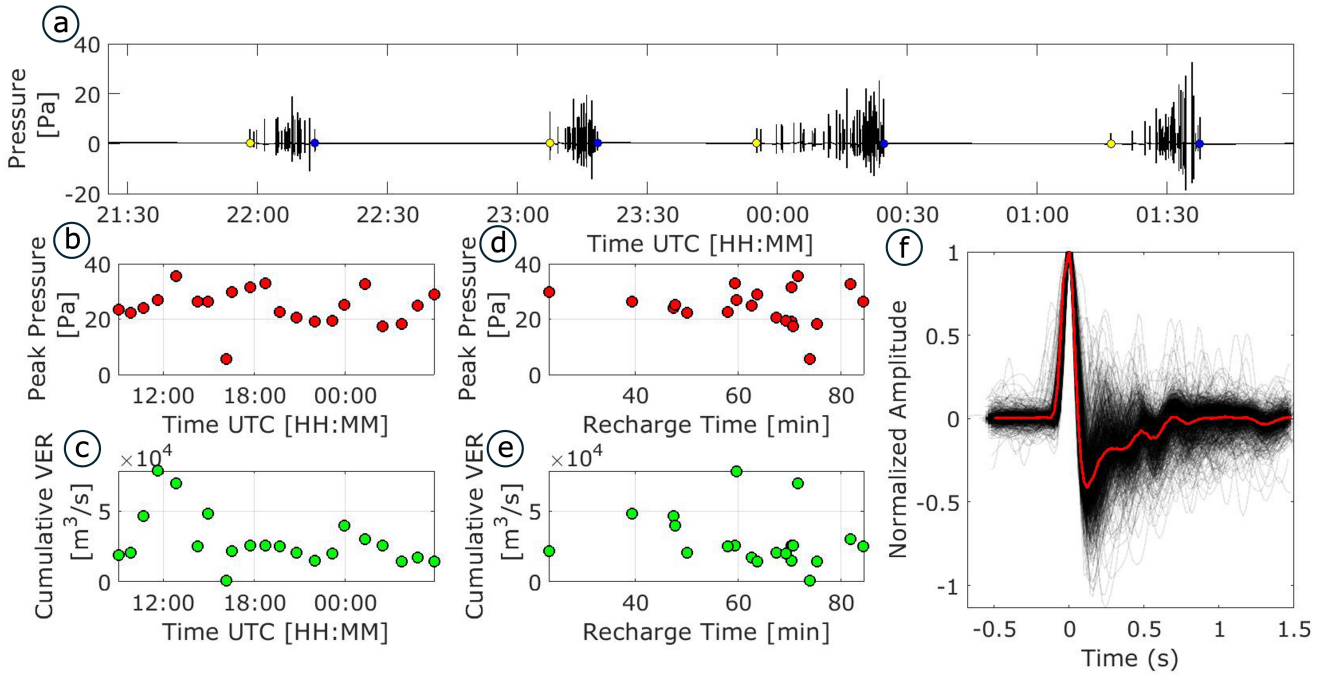


Figure 5. a) shows the discretization of each cycle. b) through e) display the peak pressure and Volcanic Explosivity Rate (VER) over time and in relation to the "recharge time". f) Waveform stacking presents the results of a 4-minute moving window analysis with a 1-minute shift, applied within each cycle to calculate both the number of explosions and their average amplitude. Time is normalized to the maximum duration of each cycle.

system[47–49]. Accordingly, we interpret the observed behavior as resulting from the partial collapse of a gas-rich foam layer at 1.5–2 km depth (Fig. 6b). In this framework, exsolved volatiles accumulate beneath a geometric barrier in the conduit until the foam becomes unstable and partially collapses, releasing gas slugs (or pockets) that drive Strombolian explosions. This mechanism is supported by laboratory experiments (e.g.[17]) and field observations at Etna (e.g.[49]), which show that a constant gas flux into an accumulation zone produces discrete, pulsatory gas release.

At shallower levels, slug ascent is likely modulated by a viscous, crystal-rich layer at the vent (Fig.6a). Infrasonic waveforms display rapid compression–rarefaction signatures characteristic of slug outbursts through a high-viscosity barrier[12]. Synchronous gas puffing and explosions from multiple SEC vents (Fig.4) further support models of plug fracturing and distributed degassing[13,14]. In these valve-like behavior, localized gas overpressure exceeds the tensile strength of the plug, creating transient fractures that open and collapse, allowing bursts of gas to escape. Progressive crystallization and cooling increase plug viscosity - and thus its strength - over each cycle, as evidenced by the rising infrasonic peak pressures in Figure 5. At SEC, we observed explosions from multiple ephemeral vents within a shallow, branching conduit system, where individual outlets respond differently to a shared gas supply. These vents are short-lived and dynamically evolve, with their eruptive behavior modulated by changes in shallow conduit conditions. In particular, variations in the degree of crystallization within the uppermost portions of these ephemeral vents likely exert a primary control on eruption style, influencing permeability, plug strength, and gas escape efficiency. Comparable dynamics have been documented at Yasur volcano, where closely spaced vents are fed by a common gas reservoir but may erupt synchronously or alternately due to shallow conduit heterogeneities and evolving magma rheology[50]. In this framework, explosions can result from the partitioning of a single gas slug into multiple pathways, with differences in timing and intensity governed by conduit geometry and the rheological state of the shallow magma column.

However, when foam accumulation and plug resistance are both overwhelmed, the entire foam layer collapses catastrophically (Fig.6b), disrupting the plug and triggering sustained lava fountaining, as commonly observed during paroxysmal episodes at Etna[47,51]. Rapid decompression drives an annular gas–pyroclast flow[3], replacing intermittent slugs with continuous explosive discharge. The 1 December paroxysm marks this transition and temporarily disrupts the shallow plumbing system.

The 2023 Etna sequence differs significantly from previously documented tremor-only cyclicity at the volcano (2008–09), which lacked surface manifestations[19]. In contrast, the 2023 cycles were clearly observable at the surface, enabling correlation of seismic and infrasound signals with eruptive dynamics.

Similar cyclic eruptions have been reported at Fagradalsfjall (Iceland, 2021), where periodic lava fountaining was linked to overpressure oscillations in a shallow magma chamber[18]. While Fagradalsfjall featured a low-viscosity lava lake allowing freer gas ascent, at Etna the viscous plug modulates gas release, producing discrete explosions and regulating cycle periodicity. In conclusion, the November–December 2023 sequence at Mt. Etna demonstrates that cyclic Strombolian activity and subsequent paroxysmal lava fountaining can be explained by coupled deep and shallow processes, including foam accumulation, slug ascent, and plug modulation. The regularity of these cycles, and their detailed seismo-acoustic signatures, provide quantitative constraints on shallow conduit dynamics and support mechanistic models of gas accumulation and release at basaltic volcanoes. Our results demonstrate that these processes are fully consistent with observations at Mount Etna, and are likely applicable to a broader class of open-vent basaltic systems. Building on this framework, our findings not only offer a robust basis for interpreting cyclic eruptive behaviour at Etna, but also provide a transferable template for monitoring and forecasting eruptive transitions at similar volcanoes. Future studies integrating high-resolution geophysical and geochemical observations with advanced modelling approaches will be essential to further refine these insights and enhance hazard assessment for communities exposed to persistent volcanic activity.

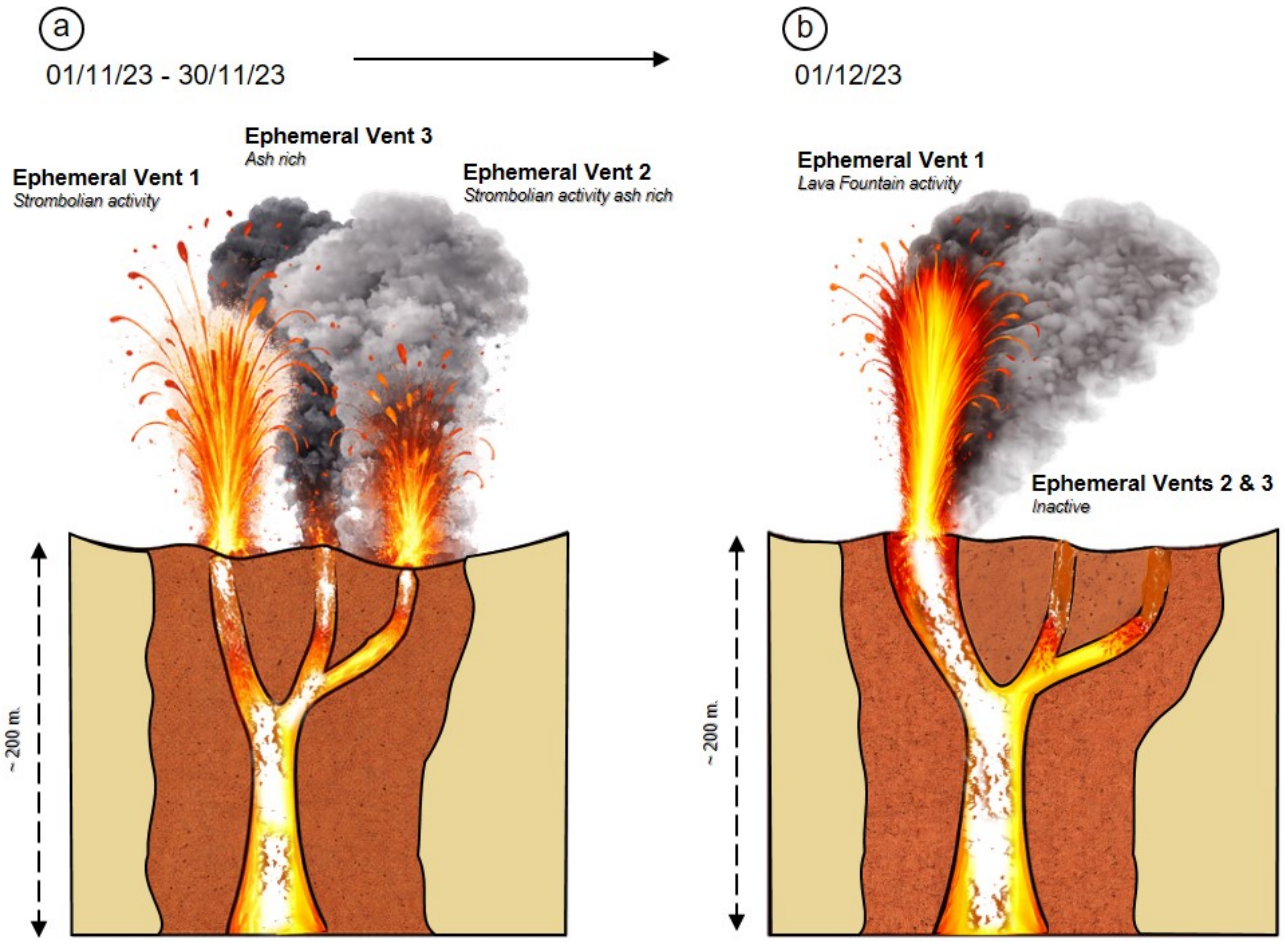


Figure 6. Conceptual model illustrating the evolution of vent configuration and shallow conduit structure over the study period. The relative sizes of the conduits are schematic and represent the volume of flux supplied to the ephemeral vents. Magma conditions within the conduit are depicted using colour gradients, ranging from hot, low-viscosity magma (yellow) to cooler, higher-viscosity magma (red to brown). Slug positions (white clouds) indicate the timing and sequence of explosive events, reflecting conduit pathway tortuosity. (A) 1–30 November: simultaneous activity at multiple ephemeral vents, characterized by ash-rich Strombolian activity; (B) 1 December: eruptive activity becomes focused at ephemeral vent 1, marked by the onset of lava fountain activity, while ephemeral vents 2 and 3 become inactive with cessation of degassing, likely promoted by increased crystallization in the shallow conduit portion, which enhanced magma viscosity and hindered gas and magma ascent toward these vents

Methods

Seismic and infrasound network

Recently on Mount Etna, an integrated seismo-acoustic network has been developed, guarantying an improvement in the monitoring system. The seismo-acoustic monitoring of Mount Etna is used to follow the magma movements beneath or within the Etna plumbing systems that could highlight an imminent volcanic eruption. The seismo-acoustic monitoring network of the INGV-OE, collects multiparametric signals to monitor the ongoing eruptive activity. The Etna eruptions are monitored by high-quality, spatial and temporal resolution multi-parametric network to allow investigating the relation between the geophysical events and the underlying processes that generate the recorded signals. In this study we analyse seismic and infrasound datasets acquired by the INGV seismo-acoustic permanent network between 20 November and 03 December 2023. The infrasonic stations are equipped with microphone G.R.A.S.® 40AN (sensibility of 50 mV/Pa), and the seismic station ECPN is equipped with a Nanometrics Trillium 40S (T=40s), 3-component seismometer. Both data at the infrasonic network and at the ECPN seismic station are digitized at 24-bit resolution with Nanometrics digitizers (50 Hz for the infrasonic stations, and 100 Hz for the seismic station), and the signals are transmitted via satellite to the data acquisition centre in real-time by INGV with a Nanometrics Trident digital system. The seismo-acoustic station ECPN is locate very close to the summit craters, at an elevation of about 3000 m a.s.l., and at distances of approximately 1000 m from active vents of SEC craters. The geometry of the infrasonic network is a ring around the summit craters at an elevation spanning 2800-3000 m a.s.l., at approximately 1000-2200 m from different active vents within the summit craters.

Seismic Tremor source location

The position of the volcanic tremor source was estimated using a grid-search method based on the decay of seismic amplitude with distance, following the procedure adopted by the seismological research group of INGV–Osservatorio Etneo (INGV-OE) for real-time monitoring of tremor activity at Mt. Etna[29,33]. Tremor source locations were computed by assuming that seismic amplitude decreases with distance according to the relation:

$$A(f,r) = A_0(f), r^{-b} e^{-\alpha r} \tag{1}$$

where f is frequency, b is an exponent equal to 0.5 and 1 for the geometric spreading related to surface and body waves, respectively, and α is the frequency-dependent attenuation coefficient defined as

$$\alpha = \frac{\pi f}{Qc} \tag{2}$$

with Q denoting the ray-path-averaged quality factor and c the seismic wave velocity. The equation is linearized by logarithmic transformation, and the coefficient of determination (R^2) of the resulting linear regression between logarithmic amplitude and source-to-station distance is used as a measure of the goodness of fit and, consequently, of location quality.

Prior to location analysis, seismic signals were band-pass filtered in the 0.5–2.5 Hz frequency range, which contains most of the volcanic tremor energy at Mt. Etna[33]. Each node of a three-dimensional grid was iteratively considered as a potential tremor source, and the R^2 value was computed for each node. The spatial distribution of R^2 values was then used to determine the tremor source location, which was assigned, at a temporal resolution of 30 minutes, to the centroid of all grid nodes (3D grid) whose R^2 values differed by no more than 1.

To assess the stability and reliability of source localization solutions, the Jackknife resampling technique[52] was performed. This method is particularly useful when the statistical distribution of the estimated parameters is unknown and when the dataset may contain influential observations. This technique is also known as the "leave-one-out" method, and it is a sequential resampling approach in which, for a dataset of n (number of stations), estimates of an unknown parameter P (e.g., latitude, longitude, and depth) are computed for each source location by omitting the i-th station at a time. These estimates are used to compute the so-called pseudovalues[33]:

$$J_i = n\hat{P} - (n-1)P_i \tag{3}$$

where $\hat{P}$ is the parameter computed by considering all the stations.

Finally, the Jackknife estimator of parameter P is given by

$$J(\hat{P}) = \frac{1}{n}\sum_{i=1}^{n} J_i = n\hat{P} - (n-1)\bar{P} \tag{4}$$

and the estimate of the standard error associated with the Jackknife estimator is given by

$$\delta_{J(\hat{P})} = \sqrt{\frac{1}{n(n-1)} \sum_{i=1}^{n} \left(J_i - J(\hat{P})\right)^2} \tag{5}$$

This standard error provides a quantitative measure of the stability of the localization results and the sensitivity of the solution to individual stations. Although the Jackknife technique is computationally demanding, it is valuable for evaluating the robustness of source parameter estimates and identifying the influence of individual observations (e.g.[29,33]). However, it does not improve the solution itself but rather provides an assessment of its stability and associated uncertainty.

Infrasound Events source location

Signal processing is carried out by independent software modules developed in-house at INGV-OE, operating continuously and automatically. Transient infrasonic signals are detected using a multi-band short-term average to long-term average (STA/LTA[53]) trigger algorithm applied across all available stations. The parameters used for the STA/LTA algorithm were as follows: (1) a band-pass filter with a frequency range of 1–6 Hz; (2) a short-term average (STA) window length of 0.5 s and a long-term average (LTA) window length of 5 s; and (3) an STA/LTA threshold of 2.8. Station-level detections are temporally associated by accounting for expected inter-station travel-time differences, allowing triggers generated by the same physical source to be merged into single network events. Event localization is performed using a grid-search approach (2D grid of 4×4 km with a spacing of 0.05 km) designed for sparse station geometries. A two-dimensional grid, coincident with summit topography and defined at fixed spatial resolution, is used to sample potential source positions. For each grid node, theoretical acoustic travel times are computed assuming straight-line propagation in a homogeneous atmosphere with constant sound speed. Event origin time is estimated from the arrival observed at a reference station selected on the basis of signal-to-noise ratio, and predicted arrival times at the remaining stations are then calculated. Waveforms are subsequently time-shifted to align signals for each hypothetical source location.

Event localization is performed using a modified version of brightness (Eq. 6)[44,54]

$$B_0 = \frac{1}{N} \sum_{i=1}^{N} \max\left(W_i\right) \tag{6}$$

where W_i is the window of the i-th signal convolved with a Hanning function:

$$W_i = \text{Hanning}\left(U_i(\tau_i + j, \Delta t)\right), \quad j = 1, \ldots, M \tag{7}$$

Here, Δt is the sampling interval, τ_i is the origin time of the window sampling the i-th channel, U_i is the signal recorded at the i-th channel, M is the number of samples in the window, and N is the number of channels.

Brightness emphasizes temporal focusing of signal energy by assessing whether peak amplitudes occur near the center of the aligned time window, making it particularly suitable for robust source localization under conditions of waveform variability.

All results are automatically integrated into the observatory database and geographic information systems, enabling near–real-time visualization and supporting continuous volcanic monitoring and hazard assessment.

Data availability

Both seismic and infrasound waveform data are part of INGV seismic network, and the data are publicly available at EIDA Italia (https://eida.ingv.it/) under Creative Commons 4.0 licensing, https://creativecommons.org/licenses/by/4.0/.

Acknowledgements

L.Z., S.D.A., are supported by SINFONIA2, progetto Bando Ricerca Libera 2024- Delibera 56/2025-INGV. L.Z., S.D.A., D.G. and M.S. by grant "Progetto INGV Pianeta Dinamico" -Sub-project VT-DYNAMO 2023- code CUP D53J19000170001 - funded by Italian Ministry MIUR ("Fondo Finalizzato al rilancio degli investimenti delle amministrazioni centrali dello Stato e allo sviluppo del Paese", legge 145/2018). S.D.A. is also supported by NERC grant NE/W004771/1. L.Z., S.D.A, D.G. and G.B. by grant ANTENNAE, funded by IX Programma Esecutivo di Cooperazione Scientifica e Tecnologica Tra la Repubblica Italiana e La Repubblica Argentina, Funded by Ministero degli Affari Esteri e della Cooperazione Internazionale (MAECI) - Ufficio XI, and by Secretaría de Innovación Ciencia y Tecnología della Repubblica Argentina - Dirección Nacional

de Planeamiento y Asuntos Internacionales de Innovación, Ciencia y Tecnología (SICYT). We thank the INGV-OE technicians for maintaining the permanent seismo-acoustic network. We also acknowledge the Seismology Unit of the INGV–Osservatorio Etneo (Catania section) for support in data management, and Dr Giuseppe Di Grazia for constructive discussions that contributed to the interpretation of Etna tremor locations.

Author contributions statement

L.Z., S.D.A. and D.G. designed the study, performed the seismic and infrasound data analyses, and prepared the figures. L.Z. drafted the manuscript, and all authors (D.G., S.D.A., M.S., and G.B.) contributed to the final version.

Funding

This research was supported by SINFONIA2, progetto Bando Ricerca Libera 2024- Delibera 56/2025-INGV; grant "Progetto INGV Pianeta Dinamico" -Sub-project VT-DYNAMO 2023- code CUP D53J19000170001 - funded by Italian Ministry MIUR ("Fondo Finalizzato al rilancio degli investimenti delle amministrazioni centrali dello Stato e allo sviluppo del Paese", legge 145/2018); by grant ANTENNAE, funded by IX Programma Esecutivo di Cooperazione Scientifica e Tecnologica Tra la Repubblica Italiana e La Repubblica Argentina, Funded by Ministero degli Affari Esteri e della Cooperazione Internazionale (MAECI) - Ufficio XI, and by Secretaría de Innovación Ciencia y Tecnología della Repubblica Argentina - Dirección Nacional de Planeamiento y Asuntos Internacionales de Innovación, Ciencia y Tecnología (SICYT).

Corresponding author

Correspondence to Luciano Zuccarello (luciano.zuccarello@ingv.it).

References

1. Andronico, D., Cristaldi, A., Del Carlo, P. & Taddeucci, J. Shifting styles of basaltic explosive activity during the 2002–03 eruption of mt. etna, italy. *J. Volcanol. Geotherm. Res.* **180**, 110–122, DOI: https://doi.org/10.1016/j.jvolgeores.2008.07.026 (2009).
2. Andronico, D., Cannata, A., Di Grazia, G. & Ferrari, F. The 1986–2021 paroxysmal episodes at the summit craters of mt. etna: Insights into volcano dynamics and hazard. *Earth-Science Rev.* **220**, 103686, DOI: https://doi.org/10.1016/j.earscirev.2021.103686 (2021).
3. Parfitt, E. A. A discussion of the mechanisms of explosive basaltic eruptions. *J. Volcanol. Geotherm. Res.* **134**, 77–107, DOI: https://doi.org/10.1016/j.jvolgeores.2004.01.002 (2004).
4. Pompilio, M., Bertagnini, A., Del Carlo, P. & Di Roberto, A. Magma dynamics within a basaltic conduit revealed by textural and compositional features of erupted ash: The december 2015 mt. etna paroxysms. *Sci. reports* **7**, DOI: https://doi.org/10.1038/s41598-017-05065-x (2017).
5. La Spina, G. *et al.* Explosivity of basaltic lava fountains is controlled by magma rheology, ascent rate and outgassing. *Earth Planet. Sci. Lett.* DOI: https://doi.org/10.1016/j.epsl.2020.116658 (2021).
6. Branca, S. & Carlo, P. D. Types of eruptions of etna volcano ad 1670–2003: implications for short-term eruptive behaviour. *Bull. Volcanol.* **67**, 732–742 (2005).
7. Cassidy, M., Manga, M., Cashman, K. & Bachmann, O. Controls on explosive-effusive volcanic eruption styles. *Nat. communications* **9**, 2839, DOI: https://doi.org/10.1038/s41467-018-05293-3 (2018).
8. Harris, A. J. & Rowland, S. K. Lava flows and rheology. In *The encyclopedia of volcanoes*, 321–342 (Elsevier, 2015).
9. Taddeucci, J., Edmonds, M., Houghton, B., James, M. R. & Vergniolle, S. Hawaiian and strombolian eruptions. In *The encyclopedia of volcanoes*, 485–503, DOI: https://doi.org/10.1016/B978-0-12-385938-9.00027-4 (Elsevier, 2015).
10. Zuccarello, L. *et al.* Geophysical fingerprint of the 4–11 july 2024 eruptive activity at stromboli volcano, italy. *Nat. Hazards Earth Syst. Sci.* **25**, 2317–2330, DOI: https://doi.org/10.5194/nhess-25-2317-2025 (2025).
11. Wallis, G. B. *One-dimensional two-phase flow* (Courier Dover Publications, 2020).
12. Del Bello, E. *et al.* Viscous plugging can enhance and modulate explosivity of strombolian eruptions. *Earth Planet. Sci. Lett.* **423**, 210–218, DOI: https://doi.org/10.1016/j.epsl.2015.04.034 (2015).
13. Suckale, J., Keller, T., Cashman, K. V. & Persson, P.-O. Flow-to-fracture transition in a volcanic mush plug may govern normal eruptions at stromboli. *Geophys. research letters* **43**, 12–071, DOI: https://doi.org/10.1002/2016GL071501 (2016).

14. Barth, A., Edmonds, M. & Woods, A. Valve-like dynamics of gas flow through a packed crystal mush and cyclic strombolian explosions. *Sci. Reports* **9**, 821, DOI: https://doi.org/10.1038/s41598-018-37013-8 (2019).

15. Vergniolle, S. & Jaupart, C. Separated two-phase flow and basaltic eruptions. *J. Geophys. Res. Solid Earth* **91**, 12842–12860, DOI: https://doi.org/10.1029/JB091iB12p12842 (1986).

16. Gonnermann, H. M., Manga, M. & Fagents, S. A. Dynamics of magma ascent in the volcanic conduit. *Model. volcanic processes: The physics mathematics volcanism* 55–84 (2013).

17. Jaupart, C. & Vergniolle, S. The generation and collapse of a foam layer at the roof of a basaltic magma chamber. *J. Fluid Mech.* **203**, 347–380, DOI: https://doi.org/10.1017/S0022112089001497 (1989).

18. Scott, S. *et al.* Near-surface magma flow instability drives cyclic lava fountaining at fagradalsfjall, iceland. *Nat. Commun.* **14**, 6810, DOI: https://doi.org/10.1038/s41467-023-42569-9 (2023).

19. Cannata, A. *et al.* New insights into banded tremor from the 2008–2009 mount etna eruption. *J. Geophys. Res. Solid Earth* **115**, DOI: https://doi.org/10.1029/2009JB007120 (2010).

20. Palacios, P. B., Díez, M., Kendall, J.-M. & Mader, H. M. Seismic-acoustic energy partitioning during a paroxysmal eruptive phase of tungurahua volcano, ecuador. *Geophys. J. Int.* **205**, 1900–1915, DOI: https://doi.org/10.1093/gji/ggw136 (2016).

21. Istituto Nazionale di Geofisica e Vulcanologia, sezione di Catania - Osservatorio Etneo. Bollettini settimanali e multidisciplinari (2023). Accessed: 2026-03-19.

22. McNutt, S. *et al.* Local seismic and infrasound observations of the 2009 explosive eruptions of redoubt volcano, alaska. *J. Volcanol. Geotherm. Res.* **259**, 63–76, DOI: https://doi.org/10.1016/j.jvolgeores.2013.03.016 (2013).

23. Eibl, E. P. S. *et al.* Multiple coincident eruptive seismic tremor sources during the 2014–2015 eruption at holuhraun, iceland. *J. Geophys. Res. Solid Earth* **122**, 2972–2987, DOI: https://doi.org/10.1002/2016JB013892 (2017).

24. Roman, D. C. Automated detection and characterization of harmonic tremor in continuous seismic data. *Geophys. Res. Lett.* **44**, 6065–6073, DOI: https://doi.org/10.1002/2017GL073715 (2017).

25. Cardone, M. *et al.* Changing magma recharge/discharge dynamics during the 2020–22 lava fountaining activity at mt. etna revealed by tilt deformation and volcanic tremor. *J. Volcanol. Geotherm. Res.* **449**, 108074, DOI: 10.1016/j.jvolgeores.2024.108074 (2024).

26. Corsaro, R. A., Miraglia, L., Arienzo, I. *et al.* The 2020–2022 paroxysmal episodes of the south-east crater (mt. etna): insights into high-frequency eruptive activity from petrological monitoring. *Bull. Volcanol.* **86**, 85, DOI: 10.1007/s00445-024-01770-4 (2024).

27. Andronico, D., D'Oriano, C., Pardini, F. *et al.* The 23–24 march 2021 lava fountain at mt etna, italy. *Bull. Volcanol.* **86**, 56, DOI: 10.1007/s00445-024-01745-5 (2024).

28. Cannata, A. *et al.* Multi-disciplinary reconstruction of magma dynamics during the 2020–22 paroxysmal sequence at mt. etna volcano. In *International Conference / Poster* (2024).

29. Di Grazia, G., Falsaperla, S. & Langer, H. Volcanic tremor location during the 2004 mount etna lava effusion. *Geophys. research letters* **33**, DOI: https://doi.org/10.1029/2005GL025177 (2006).

30. Carbone, D., Currenti, G. & Del Negro, C. Multiobjective genetic algorithm inversion of ground deformation and gravity changes spanning the 1981 eruption of etna volcano. *J. Geophys. Res. Solid Earth* **113**, DOI: https://doi.org/10.1029/2006JB004917 (2008).

31. Cannata, A. *et al.* Pressurization and depressurization phases inside the plumbing system of mount etna volcano: Evidence from a multiparametric approach. *J. Geophys. Res. Solid Earth* **120**, 5965–5982, DOI: https://doi.org/10.1002/2015JB012227 (2015).

32. Patanè, D., Di Grazia, G., Cannata, A., Montalto, P. & Boschi, E. Shallow magma pathway geometry at mt. etna volcano. *Geochem. Geophys. Geosystems* **9**, DOI: https://doi.org/10.1029/2008GC002131 (2008).

33. Cannata, A. *et al.* Monitoring seismo-volcanic and infrasonic signals at volcanoes: Mt. etna case study. *Pure Appl. Geophys.* **170**, 1751–1771, DOI: DOIhttps://doi.org/10.1007/s00024-012-0634-x (2013).

34. Viccaro, M., Zuccarello, F., Cannata, A., Palano, M. & Gresta, S. How a complex basaltic volcanic system works: Constraints from integrating seismic, geodetic, and petrological data at mount etna volcano during the july–august 2014 eruption. *J. Geophys. Res. Solid Earth* **121**, 5659–5678, DOI: https://doi.org/10.1002/2016JB013164 (2016).

35. Behncke, B., Branca, S., Corsaro, R. A., De Beni, E. & Miraglia, L. The 2011–2012 summit eruptions of mount etna: Eruptive style and structural setting. *J. Volcanol. Geotherm. Res.* **270**, 10–21, DOI: 10.1016/j.jvolgeores.2013.11.012 (2014).

36. Marchetti, E., Ripepe, M., Ulivieri, G., Caffo, S. & Privitera, E. Infrasonic evidences for branched conduit dynamics at mt. etna volcano, italy. *Geophys. Res. Lett.* **36**, DOI: https://doi.org/10.1029/2009GL040070 (2009).

37. Bonaccorso, A., Aloisi, M. & Mattia, M. Dike emplacement forerunning the etna july 2001 eruption modeled through continuous tilt and gps data. *Geophys. Res. Lett.* **29**, 2–1–2–4, DOI: https://doi.org/10.1029/2001GL014397 (2002).

38. Castro-Melgar, I., Prudencio, J., Del Pezzo, E., Giampiccolo, E. & Ibáñez, J. M. Shallow magma storage beneath mt. etna: Evidence from new attenuation tomography and existing velocity models. *J. Geophys. Res. Solid Earth* **126**, DOI: https://doi.org/10.1029/2021JB022094 (2021).

39. Corsaro, R. A. & Miraglia, L. Dynamics of 2004–2005 mt. etna effusive eruption as inferred from petrologic monitoring. *Geophys. Res. Lett.* **32**, DOI: https://doi.org/10.1029/2005GL022347 (2005).

40. Palano, M., Viccaro, M., Zuccarello, F. & Gresta, S. Magma transport and storage at mt. etna (italy): A review of geodetic and petrological data for the 2002–03, 2004 and 2006 eruptions. *J. Volcanol. Geotherm. Res.* **347**, 149–164, DOI: https://doi.org/10.1016/j.jvolgeores.2017.09.009 (2017).

41. Aiuppa, A. *et al.* Patterns in the recent 2007–2008 activity of mount etna volcano investigated by integrated geophysical and geochemical observations. *Geochem. Geophys. Geosystems* **11**, DOI: https://doi.org/10.1029/2010GC003168 (2010).

42. Ripepe, M. *et al.* Volcanic infrasound: A review. *J. Volcanol. Geotherm. Res.* **255**, 121–137, DOI: 10.1016/j.jvolgeores.2013.02.006 (2013).

43. De Angelis, S., Diaz-Moreno, A. & Zuccarello, L. Recent developments and applications of acoustic infrasound to monitor volcanic emissions. *Remote. sensing* **11**, 1302, DOI: https://doi.org/10.3390/rs11111302 (2019).

44. Kao, H. & Shan, S.-J. The source-scanning algorithm: mapping the distribution of seismic sources in time and space. *Geophys. J. Int.* **157**, 589–594, DOI: 10.1111/j.1365-246X.2004.02276.x (2004).

45. Lacanna, G. & Ripepe, M. Modeling the acoustic flux inside the magmatic conduit by 3d-fdtd simulation. *J. Geophys. Res. Solid Earth* **125**, e2019JB018849, DOI: https://doi.org/10.1029/2019JB018849 (2020).

46. De Angelis, S., Zuccarello, L., Scollo, S. & Mereu, L. Assessment of eruption source parameters using infrasound and plume modelling: a case study from the 2021 eruption of mt. etna, italy. *Sci. Reports* **13**, 19857, DOI: https://doi.org/10.1038/s41598-023-46160-6 (2023).

47. Allard, P., Burton, M. & Muré, F. Spectroscopic evidence for a lava fountain driven by previously accumulated magmatic gas. *Nature* **433**, 407–410, DOI: 10.1038/nature03246 (2005).

48. Spilliaert, N., Allard, P., Métrich, N. & Sobolev, A. V. Magma degassing and generation of basaltic pyroclastic activity at mount etna, italy: insights from gas composition and melt inclusions. *J. Volcanol. Geotherm. Res.* **159**, 143–160, DOI: 10.1016/j.jvolgeores.2006.06.006 (2006).

49. Carbone, D., Zuccarello, L., Messina, A., Scollo, S. & Rymer, H. Balancing bulk gas accumulation and gas output before and during lava fountaining episodes at mt. etna. *Sci. reports* **5**, 18049, DOI: https://doi.org/10.1038/srep18049 (2015).

50. Simons, B., Jolly, A., Eccles, J. & Cronin, S. Spatiotemporal relationships between two closely-spaced strombolian-style vents, yasur, vanuatu. *Geophys. Res. Lett.* **47**, e2019GL085687, DOI: https://doi.org/10.1029/2019GL085687 (2020).

51. Andronico, D., Scollo, S., Caruso, S. & Cristaldi, A. The 2010–2011 explosive activity at mt. etna: eruption chronology and eruption dynamics. *J. Geophys. Res. Solid Earth* **118**, 2803–2821 (2013).

52. Efron, B. The jackknife, the bootstrap and other resampling plans. In *CBMS-NSF Regional Conference Series*, DOI: http://dx.doi.org/10.1137/1.9781611970319 (Applied Mathematics, Monograph 38, SIAM, Philadelphia, 1882).

53. Withers, M. *et al.* A comparison of select trigger algorithms for automated global seismic phase and event detection. *Bull. Seismol. Soc. Am.* **88**, 95–106, DOI: 10.1785/BSSA0880010095 (1998).

54. Cannata, A. *et al.* Clustering and classification of infrasonic events at mount etna using pattern recognition techniques. *Geophys. J. Int.* **185**, 253–264, DOI: https://doi.org/10.1111/j.1365-246X.2011.04951.x (2011).

Supplementary Material

We present supplementary figure accompanying the main text that provide visual documentation of the 2023 eruptive activity of Mount Etna, focusing on three ephemeral vents within the South East Crater (Figures S1). Additionally, Figure S2 illustrates the variations in the mean amplitudes of the recorded explosions during the study period.

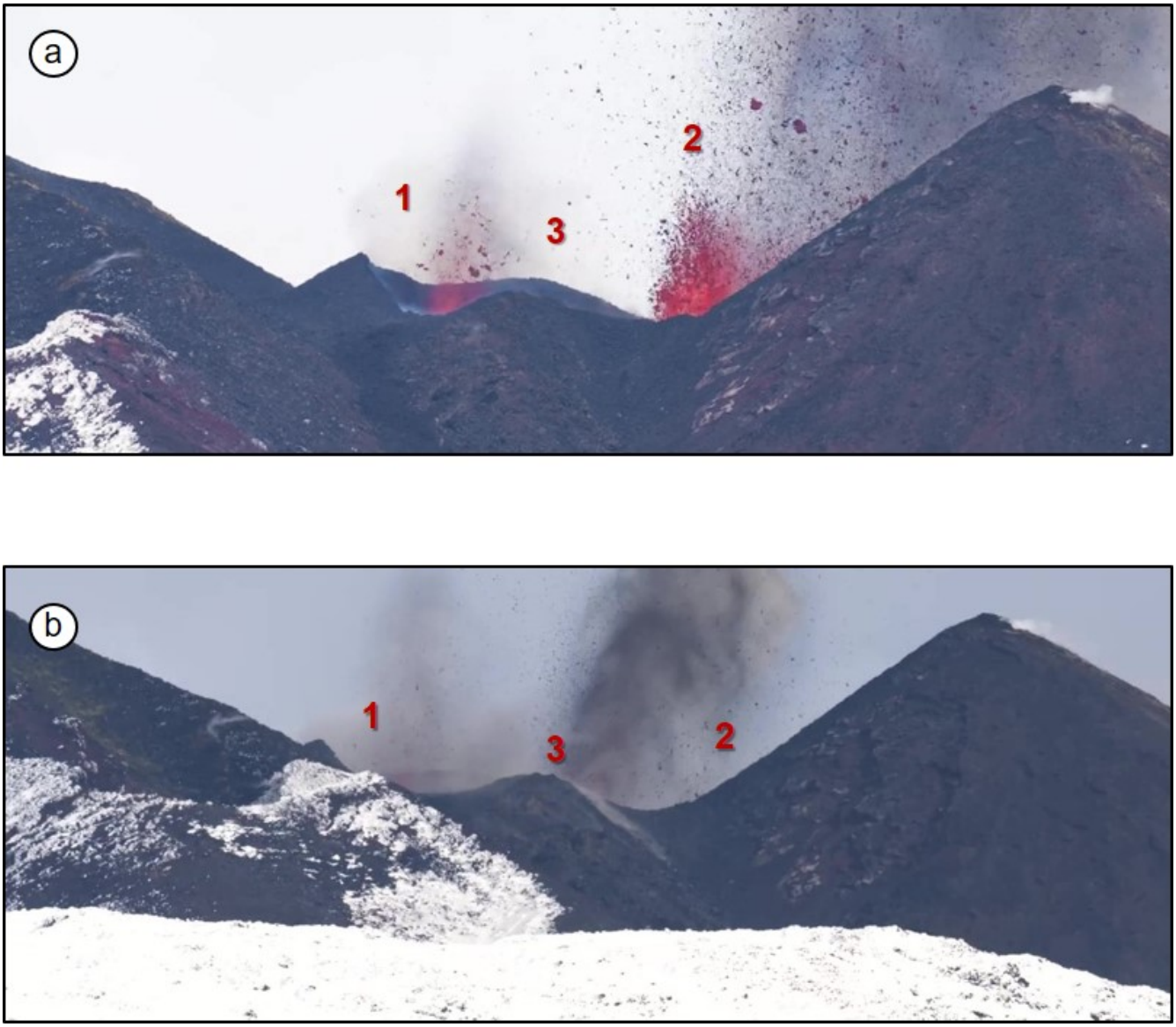


Figure S1. Images of the South East Crater documenting eruptive activity at three ephemeral vents (1, Ephemeral Vent 1; 2, Ephemeral Vent 2; 3, Ephemeral Vent 3), occurring in a near-synchronous manner. Photo (a) shows simultaneous explosive activity at ephemeral vents 1 and 3, whereas photo (b) illustrates ongoing eruptive activity at ephemeral vent 3 alongside the partial cessation of explosive activity at ephemeral vent 1 (photo credit: M. Mammino).

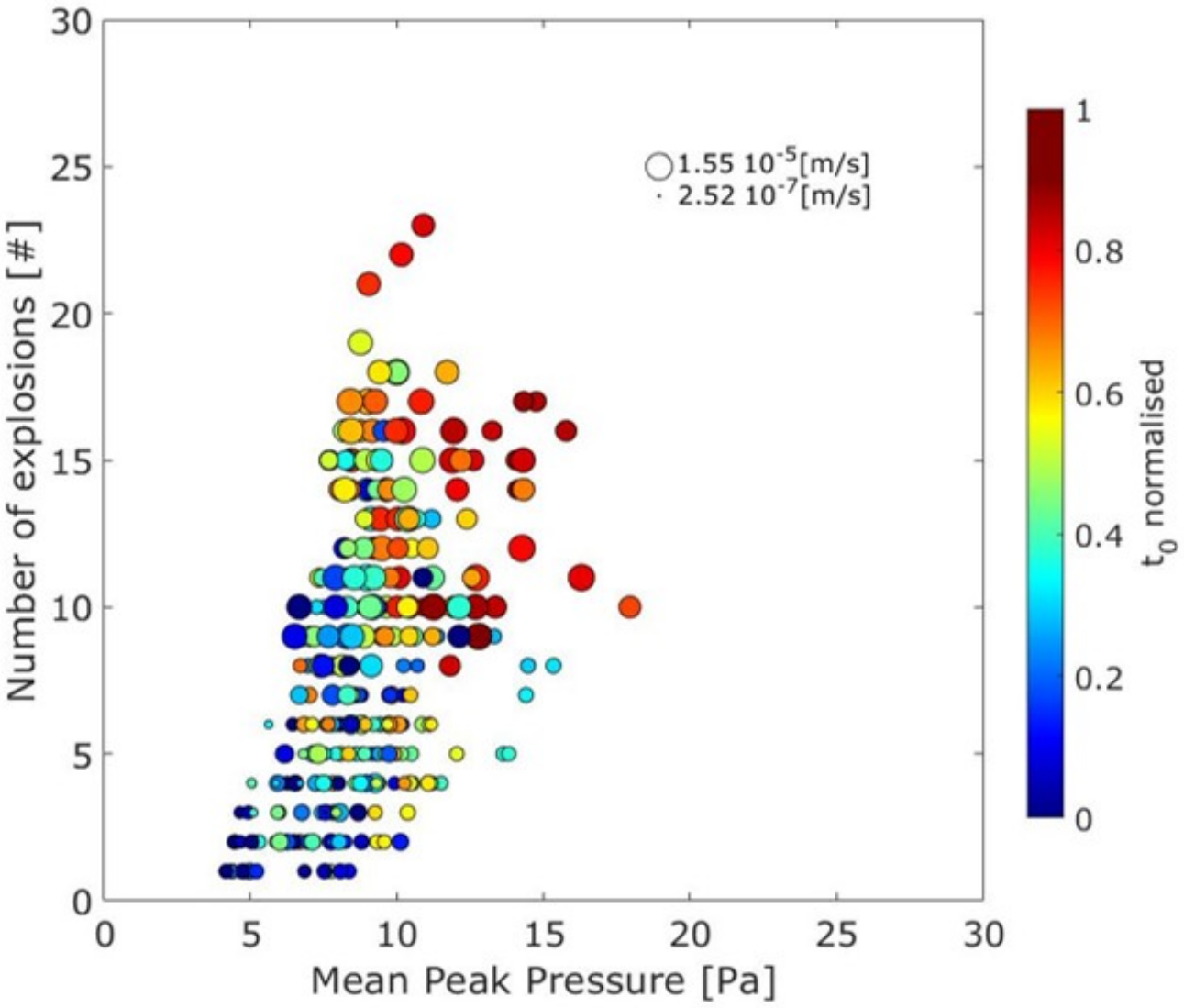


Figure S2. The results of a 4-minute moving window analysis with a 1-minute shift, applied within each cycle to calculate both the number of explosions and their average amplitude. Each dot represents one window, with the x-axis showing the mean peak pressure, and the y-axis indicating the number of explosions. Dot size is scaled by the RSAM amplitude of the seismic signal in the corresponding window, and the color represents normalized time within the cycle (from 0 at the cycle onset to 1 at the end).

Supplementary Files

This is a list of supplementary files associated with this preprint. Click to download.

- SupplementaryMaterial.pdf